

**Kinetic Monte Carlo approach to modeling thermal decay in perpendicular recording media**T. J. Fal,<sup>1</sup> J. I. Mercer,<sup>2</sup> M. D. Leblanc,<sup>1</sup> J. P. Whitehead,<sup>1</sup> M. L. Plumer,<sup>1</sup> and J. van Ek<sup>3</sup><sup>1</sup>*Department of Physics and Physical Oceanography, Memorial University of Newfoundland, St. John's, NL, Canada, A1B 3X7*<sup>2</sup>*Department of Computer Science, Memorial University of Newfoundland, St. John's, NL, Canada, A1B 3X7*<sup>3</sup>*Western Digital Corporation, San Jose, California 94588, USA*

(Received 9 October 2012; revised manuscript received 3 December 2012; published 6 February 2013)

A procedure is developed to study the evolution of high anisotropy magnetic recording media due to thermally activated grain reversal. It is assumed that the system is composed of single domain grains that evolves by passing through a sequence of relatively long-lived metastable states punctuated by abrupt reversals of individual grains. Solutions to the rate equations describing the sequence of metastable states are calculated using kinetic Monte Carlo. Transition rates are formulated from the Arrhenius-Néel expression in terms of the material parameters, temperature, and applied field. Results obtained from this method are shown to be in good agreement with those calculated from finite-temperature micromagnetics. The method is applied to study the rate dependence of finite-temperature  $MH$  loops and the thermal degradation of a recorded bit pattern in perpendicular recording media. A significant advantage of the procedure is its ability to extend simulations over time intervals many orders of magnitude greater than is feasible using standard finite-temperature micromagnetics with relatively modest computational effort.

DOI: [10.1103/PhysRevB.87.064405](https://doi.org/10.1103/PhysRevB.87.064405)

PACS number(s): 75.50.Ss, 75.78.Cd, 75.40.Mg

**I. INTRODUCTION**

The continued increase in the areal density of magnetic storage media has resulted from a number of remarkable advances in the technologies used to record, read back, and store data at increasingly smaller length scales.<sup>1</sup> Modern magnetic recording media is characterized by nanometer-scale, weakly interacting grains of volume composed of Co-based alloys with magnetic properties that are dominated by high perpendicular uniaxial anisotropy. Principal limiting factors on bit-size reduction involve the competition between the recordability of well-defined bits, which is characterized by the media transition signal-to-noise ratio (SNR), and long-term thermal stability.<sup>2</sup> Whereas the energy barrier to grain reversal,  $\Delta E \sim KV$ , needs to be small for recording good transitions, the anisotropy and grain volume need to be large to ensure robustness against superparamagnetic fluctuations. The introduction of perpendicular magnetic recording (PMR) in 2006 helped alleviate these issues.<sup>3</sup> More recently, exchange coupled composite (ECC) media, composed of layers with varying anisotropy strengths, have brought further advances in making bits smaller and stable with acceptable SNR.<sup>4</sup> Further technical refinements of these recent paradigms will continue to bring incremental improvements but new technologies are being actively pursued, such as heat assisted magnetic recording<sup>5–7</sup> and bit patterned media.<sup>8</sup> In addition to significant advances in materials science and fabrication techniques, numerical modeling of the recording process has played a crucial role in the realization of areal density increases in recent decades<sup>9</sup> and continues to be a key part of the evaluation of new technologies.

The starting point for many models of granular media is the description of the individual grains in terms of the Stoner-Wohlfarth (SW) model.<sup>10</sup> Grains are treated as single-domain particles in an applied field  $\vec{H}$  with a uniaxial anisotropy. The effects of the intergranular interactions may be included by combining the energy of an ensemble of Stoner-Wohlfarth particles (SWPs) with the exchange and magnetostatic inter-

action energies between the grains. This yields the effective fields  $\vec{H}_i^{\text{eff}} = -\partial E/\partial \vec{m}_i$  which can be incorporated into the Landau-Lifschitz-Gilbert (LLG) equation that is widely used to model the dynamics of magnetic media. This formalism can be extended to finite temperature with the introduction of a stochastic “thermal field” as described by Brown.<sup>11</sup> However, integrating the LLG simulations typically requires time steps on the order of picoseconds and even with the current generation of computers, it is not feasible to use the LLG simulations to model phenomena with time scales greater than 10–100 ms.<sup>12</sup> Therefore using short-time LLG simulations to estimate model parameters obtained from room-temperature long-time-scale (minutes to hours)  $MH$  loops, using standard vibrating sample magnetometry (VSM), cannot be considered reliable. Likewise the LLG simulations cannot be directly employed to study recorded bit decay due to thermally assisted grain reversal on time scales of interest for magnetic recording media that extend to years.

Efforts to overcome this problem using a scaling theory based on the Arrhenius-Néel law, which provides for an equivalence between the time and temperature, in the LLG simulations have been explored. This allows for results obtained from LLG simulations at elevated temperatures and ms time scales to be extrapolated to much longer times scales at lower (e.g., room) temperature.<sup>13</sup> The method is predicated on the assumption that the time scale associated with thermally assisted reversal may be characterized within the underlying approximations of the Arrhenius-Néel formulation, with an energy barrier and attempt frequency that are temperature independent. This method has been applied to study both the rate dependence of  $MH$  loops<sup>13</sup> and the bit decay<sup>14</sup> caused by thermal fluctuations in the case of simple single-layer longitudinal media designs.

Another approach to model long-term thermally assisted reversal has been the use of rate equations to study the time dependence of the probability distribution of the grains among their minimum-energy states, with the transition rates for the individual grains expressed in terms of an Arrhenius-Néel law.

In the case of grains with a uniaxial anisotropy, the energy minima and the barriers separating them may be calculated from the Stoner-Wohlfarth energy. This approach was used by Sharrock<sup>15</sup> to determine the remanent coercivity  $H_{cr}(t)$  of an ensemble of noninteracting SWPs. This provided one of the earliest quantitative estimates of the role of kinetic effects on the finite temperature coercivity of magnetic recording media. There have been a number of semianalytic reformulations of Sharrock's Law to extend its applicability. However, a recent comparison between one such reformulation<sup>16</sup> and a finite-temperature LLG simulation showed that, while it was able to provide a reasonable description of the rate dependence of the coercive field calculated using the LLG simulations for single layer PMR media in a perpendicular field, at fields of  $45^\circ$  and for dual layer ECC media it gave unphysical values for the attempt frequency  $f_0$  and could not reproduce the global scaling.<sup>12</sup>

In the past, rate equations have also been used with some considerable success in modeling the thermal decay of a bit pattern in longitudinal media and the remanent coercivity using a mean-field approach, in which the longitudinal component of the magnetostatic field is evaluated self-consistently.<sup>17,18</sup> From this the magnetic state is calculated as a function of time from the numerical integration of the rate equations. Results presented for several film thicknesses were shown to be in good agreement with experimental measurements. We note, however, that this mean-field approach relies on an averaging over the hundreds of grains that were in a bit typical for longitudinal media at that time and, as a mean-field model, cannot be used to estimate the noise contribution to SNR. Typical recorded bits today involve only a few dozen grains.

In this paper we study the problem of thermally assisted grain reversal in PMR media using a variant of the kinetic Monte Carlo (KMC) algorithm referred to as the first reaction method (FRM<sup>19</sup>) due to Gillespie<sup>20</sup> in which the time between successive reversals is calculated based on the Arrhenius-Néel expression for the transition rates between the minimum-energy states of the individual grains. The minimum-energy states of the grains and the energy barriers separating them are calculated using analytical expressions which give solutions for all extrema in the energy landscape for SWPs in an external magnetic field.<sup>21</sup> To account for magnetostatic and exchange interactions between the grains the SW energy is modified to include the effective fields and the magnetostatic shape anisotropy of the grains.

Kinetic Monte Carlo algorithms have been shown to be very effective in modeling the thermally activated processes in a wide range of phenomena in both physics and chemistry<sup>22-27</sup> (in chemistry the method is often referred to as dynamic Monte Carlo). While a variant of KMC based on another algorithm due to Gillespie<sup>20,28</sup> has been applied to study thermally activated processes primarily in longitudinal media,<sup>29-33</sup> it has not been as widely used in modeling the properties of PMR media as one might expect. While the KMC algorithm used in these earlier works is closely related to the FRM variant used in the present work, the FRM algorithm is more appropriate for systems in which the transition rates are time dependent.<sup>22,23</sup>

In many previous studies of thermally assisted grain reversal based on the Arrhenius-Néel expression, the attempt frequency  $f_0$  is explicitly or implicitly assumed to be constant. Typically

a value of  $f_0 \approx 1-10$  GHz is assumed,<sup>34-36</sup> consistent with experimental measurements on Co nanoparticles.<sup>37</sup> While the transition rate is far less sensitive to the attempt frequency than it is to the energy barrier, it has been shown by a number of authors to be both field and temperature dependent<sup>34,38,39</sup> and can range in value  $1 \text{ GHz} \lesssim f_0 \lesssim 50 \text{ GHz}$ ,<sup>39</sup> and can be important in interpreting results from experimental studies.<sup>40</sup> As we will show, it is straightforward to incorporate the field and temperature dependence of the attempt frequency into the KMC algorithm. This allows us to make a direct comparison with results obtained using KMC with those obtained from a stochastic LLG simulations with no adjustable parameters.

We apply KMC<sup>41</sup> to study the decay of a uniformly magnetized film both with and without interactions. The results are compared with analytical formulations in the case of noninteracting grains and with finite-temperature LLG simulations in the case of interacting grains. The agreement is shown to be very good. The method is also applied to study the SNR decay of a bit pattern in perpendicular magnetic recording media and the field sweep rate dependence of finite-temperature  $MH$  loops. In the case of the  $MH$  loops, the results are compared to those obtained from the LLG simulations and are shown to be in good agreement for low sweep rates. The obvious benefit of KMC is that it allows us to evaluate the thermally activated decay of PMR media over much longer times than is feasible using the stochastic LLG simulations.

The paper is laid out as follows. In Sec. II we describe the method for calculating the wait time for an ensemble of noninteracting SWPs and show how it may be used to calculate the evolution of the net magnetization due to thermally assisted grain reversal. The method is then applied to calculate the remanent coercivity of an ensemble of noninteraction SWPs. In Sec. III the method is extended to include the effect of the interparticle interaction through the introduction of the effective fields that account for exchange and magnetostatic interactions. The method is then applied to study the decay of the magnetization of a uniformly magnetized film in a reverse field and the results are compared with those obtained using the LLG simulations. Sections IV and V present results for SNR decay of a bit pattern and the rate dependence of finite-temperature  $MH$  loops calculated using KMC, respectively. In the case of the finite-temperature  $MH$  loops, the results of the Monte Carlo simulations are compared with those obtained from the finite-temperature LLG simulations. We finish with some concluding remarks and discuss ways in which the method may be improved and generalized to consider more complex magnetic media.

## II. REMANENT COERCIVITY

In this section KMC is applied to simulate thermally assisted grain reversal in high anisotropy PMR media. To demonstrate the method we begin by evaluating the wait time for an ensemble of noninteracting SWPs in a uniform applied field  $\vec{H}$  and calculate the remanent coercivity  $H_{cr}(t_0)$ , defined as the reverse field required to reduce the remanent magnetization to zero in time  $t_0$ . The results are compared with analytical formulations<sup>15</sup> and with those obtained from the direct integration of the rate equation.

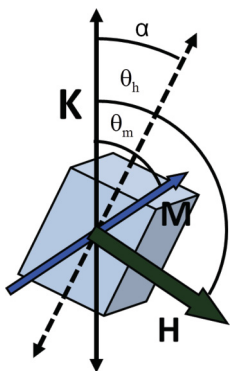


FIG. 1. (Color online) Schematic diagram showing the relative alignment of the anisotropy axis, field, and magnetic moment.

The energy of a SWP of volume  $V$  with a saturation magnetization  $M_s$ , uniaxial anisotropy of strength  $K$ , in a magnetic field  $\vec{H}$  may be written<sup>10</sup>

$$E = -VK(\hat{n} \cdot \hat{m})^2 - \mu_0 VM_s \vec{H} \cdot \hat{m}, \quad (1)$$

where  $\hat{n}$  denotes the direction of the crystal anisotropy axis and  $\hat{m}$  the direction of the magnetization. The relative alignment of the crystal anisotropy axis, applied field, and the magnetic moment are shown in Fig. 1.

In equilibrium the magnetic moment of the SWP will align such that there is zero effective field acting on it  $\partial E / \partial m_\alpha = 0$ , where  $\alpha = x, y, \text{ or } z$  directions, with stable configurations corresponding to a minimization of the energy. The energy minima lie in the plane formed by the applied field vector and crystal anisotropy axis, which may be expressed as a function of  $\theta_m$  (see Fig. 1),

$$E_{SW} = -VK \cos(\theta_m)^2 - \mu_0 VM_s H \cos(\theta_m - \theta_h). \quad (2)$$

The roots of the derivative  $dE_{SW}/d\theta_m$  are given by<sup>21</sup>

$$\cos \theta_m = \frac{f}{6} \pm \frac{1}{6} \sqrt{2f^2 - 18e + \frac{54h_2(1+h_1^2)}{f}} - \frac{h_2}{2}, \quad (3)$$

where the reduced field  $\vec{h} = \mu_0 M_s \vec{H} / 2K$ , with  $h_1 = h \cos \theta_h$  and  $h_2 = h \sin \theta_h$ , and  $e$  and  $f$  are defined as

$$e = (1 - h^2) \cos \left( \frac{1}{3} \cos^{-1} \left[ \frac{54h_1^2 h_2^2}{(1 - h^2)^3} \right] \right), \quad (4)$$

$$f = \pm \sqrt{9h_2^2 + 6(1 - h^2) + 6e}. \quad (5)$$

For low-field values the derivative  $dE_{SW}/d\theta_m$  has four real roots, two that minimize the energy and two that maximize the energy. As the magnitude of the applied field  $h$  is increased two of the roots coalesce. This defines the switching field  $h_s$ . For  $h > h_s$  the derivative  $dE_{SW}/d\theta_m$  has two real roots, one that maximizes the energy and the other that minimizes the energy. A parametric plot of the components of the switching field  $\vec{h}_s$  as a function of  $\theta_h$  defines the well-known Stoner-Wohlfarth astroid.<sup>10</sup>

Consider now a film consisting of  $N$  single domain grains with the crystal anisotropy axes aligned perpendicular to the plane of the film, which we define as the  $z$  axis. A uniform magnetic field  $\vec{H}$  is applied to the film with  $H_z < 0$  and  $|\vec{H}| < H_s$ . The magnetic moment of the grains will therefore have two

stable minima, one with  $m_z = \hat{m}_\uparrow \cdot \hat{z} > 0$  which we denote as “spin up” and a second with  $m_z = \hat{m}_\downarrow \cdot \hat{z} < 0$  which we denote as “spin down.” Denoting by  $r_{\uparrow\downarrow}$  ( $r_{\downarrow\uparrow}$ ) the transition rate from the spin up to spin down (spin-down to spin-up) state, the rate equations describing the evolution of the probability of particles in the spin-up and the spin-down states, which we denote as  $P_\uparrow$  and  $P_\downarrow$ , respectively, can be written as

$$\frac{dP_\uparrow}{dt} = -r_{\uparrow\downarrow} P_\uparrow + r_{\downarrow\uparrow} P_\downarrow, \quad (6)$$

$$\frac{dP_\downarrow}{dt} = -r_{\downarrow\uparrow} P_\downarrow + r_{\uparrow\downarrow} P_\uparrow. \quad (7)$$

These equations may be readily solved to yield explicit expressions for the average populations  $P_\uparrow$  and  $P_\downarrow$ ,

$$P_\uparrow(t) = r^{-1}(r_{\downarrow\uparrow} + r_{\uparrow\downarrow} e^{-rt}), \quad (8)$$

$$P_\downarrow(t) = r^{-1}(r_{\uparrow\downarrow} - r_{\downarrow\uparrow} e^{-rt}), \quad (9)$$

where we have defined  $r = r_{\uparrow\downarrow} + r_{\downarrow\uparrow}$  and have applied the initial conditions  $P_\uparrow(t=0) = 1$  and  $P_\downarrow(t=0) = 0$ . From Eqs. (8) and (9) the time dependence of the perpendicular magnetization can be expressed in terms of the transition rates  $r_{\uparrow\downarrow}$  and  $r_{\downarrow\uparrow}$  as

$$M(t) = M_s(\hat{m}_\uparrow P_\uparrow - \hat{m}_\downarrow P_\downarrow) \cdot \hat{z}. \quad (10)$$

Assuming that the transition rates are given by the Arrhenius-Néel expression, we have

$$r_{\uparrow\downarrow} = f_0 e^{-\Delta E_{\uparrow\downarrow}/k_B T}, \quad (11)$$

$$r_{\downarrow\uparrow} = f_0 e^{-\Delta E_{\downarrow\uparrow}/k_B T}, \quad (12)$$

where  $f_0$  denotes the attempt frequency and  $\Delta E_{\uparrow\downarrow}$  and  $\Delta E_{\downarrow\uparrow}$  represent the energy barriers between the two equilibrium states. All the quantities  $\hat{m}_\uparrow \cdot \hat{z}$ ,  $\hat{m}_\downarrow \cdot \hat{z}$ ,  $\Delta E_{\uparrow\downarrow}$ , and  $\Delta E_{\downarrow\uparrow}$  may be calculated from Eqs. (3)–(5) in terms of the anisotropy and field parameters. Defining  $M(t_0) \equiv 0$  we can therefore evaluate  $t_0$  for a given field to obtain the finite-temperature remanent coercivity field  $H_{cr}$  as a function of the time interval  $t_0$ .

For the particular case where the field is perpendicular to the film, the stable spin alignments are also perpendicular to the film. In this case the energy barriers are given by  $\Delta E_{\uparrow\downarrow} = V_s K [1 - \mu_0 H M_s / (2K)]^2$  and  $\Delta E_{\downarrow\uparrow} = V_s K [1 + \mu_0 H M_s / (2K)]^2$ . It is then possible to calculate  $H_{cr}$  analytically. Assuming the magnitude of the applied field is sufficiently large such that  $\Delta E_{\uparrow\downarrow} \ll \Delta E_{\downarrow\uparrow}$  then  $M/M_s \approx 1 - 2 \exp(-rt)$ . Setting  $M = 0$ , we obtain the well-known Sharrock formula for the remanent coercivity,<sup>15</sup>

$$H_{cr}(t_0) = \frac{2K}{\mu_0 M_s} \left( 1 - \sqrt{\frac{k_B T}{K V} \ln \left( \frac{f_0 t_0}{\ln 2} \right)} \right). \quad (13)$$

Results for the more general case in which the field is aligned at some angle  $\theta_h$  to the  $z$  axis are shown in Fig. 2 (discussed below). The remanent coercivity decreases as the angle between the anisotropy axis and the applied field increases as well as with increasing time interval  $t_0$ . The decrease in the remanent coercivity with increasing  $t_0$  is due to the thermally activated reversals.

Kinetic Monte Carlo, in which the decay process is modeled stochastically, provides an alternative approach to the direct

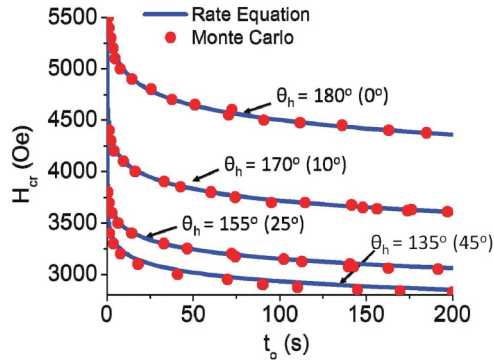


FIG. 2. (Color online) Remanent coercivity  $H_{cr}$  as a function of the time interval for a system of  $16 \times 16$  grains of dimension  $8 \text{ nm} \times 8 \text{ nm} \times 10 \text{ nm}$  with  $M_s = 5 \times 10^5 \text{ A/m}$ ,  $K = 3.75 \times 10^5 \text{ J/m}^3$ ,  $T = 330 \text{ K}$ , and  $f_0 = 1 \text{ GHz}$ . The anisotropy axis is aligned perpendicular to the plane of the film and results are presented for several values of  $\theta_h$  as indicated. The solid line is calculated by the direct integration of the rate equations while the red circles are the results obtained using KMC.

integration of the rate equations. The transition rate for each of the individual grains will be given by  $r_i = r_{\uparrow\downarrow}$  or  $r_{\downarrow\uparrow}$  depending on whether the grain is aligned in the spin-up or spin-down state. For each grain we may therefore calculate a stochastic variable  $t_i$  defined as

$$t_i = r_i^{-1} \ln x, \quad (14)$$

where  $x$  is a uniformly distributed random number  $0 < x \leq 1$ . The stochastic variable  $t_i$  describes an exponential distribution with a decay constant  $r_i$  and represents how long we typically would have to wait for the  $i$ th spin to undergo a reversal. The minimum element of the set  $\{t_i\}$  therefore denotes the time we would have to wait for the first reversal to occur. We define this quantity as the wait time  $T_w^{(1)}$  and the particular grain associated with it as the target grain. The calculation of the wait time forms the basis of the FRM.

To chart the evolution of the system for  $t > T_w^{(1)}$ , we generate the new state with the target grain reversed and assign an appropriate rate constant for each grain depending on whether it is aligned spin up,  $r_i = r_{\uparrow\downarrow}$ , or spin down,  $r_i = r_{\downarrow\uparrow}$ . A new set of stochastic variables  $\{t_i\}$  are calculated for each grain and a new wait time  $T_w^{(2)} = \min\{t_i\}$  and target grain are obtained. This represents the time interval between the first and second reversal to occur. Iterating this process yields a sequence of wait times  $T_w^{(n)}$  that give the time between successive grain reversals and the sequence of states which describe the evolution of the system. The stochastic nature of the method means that the sequence of times and states obtained will be different for each run, modeling the inherently stochastic nature of the thermally activated grain reversals of the physical system. Figure 2 shows a comparison of the results obtained using the stochastic integration technique for a  $16 \times 16$  ensemble of noninteracting grains, with  $M_s = 5 \times 10^5 \text{ A/m}$ ,  $K = 3.75 \times 10^5 \text{ J/m}^3$ ,  $T = 330 \text{ K}$ , and  $f_0 = 1 \text{ GHz}$ , together with those obtained from the direct integration of the rate equations. We note that the agreement is very good, illustrating the equivalence between stochastic integration and

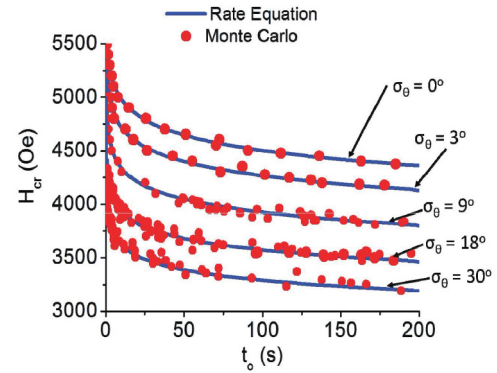


FIG. 3. (Color online) Remanent coercivity  $H_{cr}$  as a function of the time interval for the model system as in Fig. 2. The anisotropy axis is normally distributed about perpendicular to the plane of the film with variance  $\langle \alpha^2 \rangle = \sigma_\theta^2$  and results are presented for several values of  $\sigma_\theta$  as indicated. The solid line is calculated by the direct integration of the rate equations while the red circles are the results obtained using KMC.

the direct integration method for the case of noninteracting particles.

Both methods can be generalized to consider the case of an ensemble of noninteracting SWP's for which the anisotropy axis is normally distributed about the perpendicular  $z$  axis with variance  $\langle \alpha^2 \rangle = \sigma^2$  and  $\vec{H} = -H_{cr} \hat{z}$ . In the case of the direct integration method we parametrize the solutions to the rate equation given by Eq. (10) in terms of  $\alpha$ , the angle the anisotropy axis makes with the  $z$  axis (Fig. 1), as  $M(\alpha, t)$ . The net magnetization is then calculated by averaging over the probability distribution of the anisotropy angles, which we denote by  $P_K(\alpha)$ , to give

$$M(t) = \int d\alpha P_K(\alpha) M(\alpha, t). \quad (15)$$

Integrating the above expression we can calculate the root  $t_0$ , defined as  $M(t_0) = 0$ , as a function of the applied field  $H$  and variance  $\sigma^2$ . Results are presented in Fig. 3 for several values of  $\sigma$  and show that the effect of even a small variation in the direction of the anisotropy axis can have a significant effect on the remanent coercivity.

In the case of the KMC algorithm we consider, as before, a finite ensemble of  $N$  grains. In this case each grain will have a different anisotropy axis determined from the distribution  $P_K(\alpha)$ . This means that for a given spin configuration each grain will have a different rate  $r_i = f_0 \exp -\Delta E_i / k_B T$ , where  $\Delta E_i$  denotes the energy barrier separating the two energy minima of the  $i$ th grain. We then define the set of  $N$  stochastic variables  $t_i = r_i^{-1} \ln x$ , from which we obtain the wait time  $T_w^{(1)}$  and target grain as before. Iterating this procedure yields the sequence  $T_w^{(n)}$  that gives the time between successive grain reversals and the corresponding states from which the evolution of the net magnetization of the system can be evaluated as a function of time. Values of  $t_0$  calculated from the stochastic integration procedure are presented in Fig. 3. Again they show good agreement with the results obtained from the direct integration but with somewhat more scatter than the results in Fig. 2 due to the random distribution of the anisotropy axes.

The method can also be applied to consider distributions in other material parameters (e.g., magnetization, anisotropy strength, and volume).

As mentioned in the Introduction, a number of other authors have used another variant KMC to study longitudinal media.<sup>29–33</sup> In the KMC variant used in these studies the wait time is determined from the sum of the transition rates  $r = \sum_i r_i$  as  $T_w = r^{-1} \ln x$  while the target spin is selected with probability  $r_i/r$ .<sup>28</sup> While the two methods are essentially equivalent in the case of time-independent transition rates the FRM is the method of choice in the case of time-dependent transition rates.<sup>22,23</sup>

### III. INTERPARTICLE INTERACTIONS

To generalize the KMC algorithm to include interactions between the grains, the expression for the SWP energy given by Eq. (2) must be modified to include the shape anisotropy arising from the magnetostatic self-energy term and the applied field  $\vec{H}$  replaced by the effective field  $\vec{H}_i^{\text{eff}}$  that includes the effect of the magnetostatic and exchange fields between the grains. The modified energy for a single grain of cross-sectional area  $w \times w$  and thickness  $l$  is given by

$$E = -VK \sum_i (\hat{n}_i \cdot \hat{m})^2 - \frac{1}{2} \mu_0 V M_s^2 \sum_i \hat{m}_i \cdot \overleftrightarrow{N}_{ii} \cdot \hat{m}_i - \mu_0 V M_s \sum_i \vec{H}_i^{\text{eff}} \cdot \hat{m}_i, \quad (16)$$

where  $\overleftrightarrow{N}_{ij}$  denotes the magnetostatic tensor,  $\delta_i$  the nearest-neighbor sites of the  $i^{\text{th}}$  grain, and  $J = 2Aw^2/l$ , with  $A$  denoting the usual micromagnetic exchange parameter. The effective fields  $\vec{H}_i^{\text{eff}} = -\partial E_{\text{int}}/\partial \vec{m}_i$ , where  $E_{\text{int}}$  denotes the interaction energy between the grains and are given by

$$\vec{H}_i^{\text{eff}} = \vec{H} - M_s \sum_{j \neq i} \overleftrightarrow{N}_{ij} \cdot \vec{m}_j + J/(\mu_0 V M_s) \sum_{\delta_i} \hat{m}_{\delta_i}. \quad (17)$$

The components of the magnetostatic self-energy term may be written as  $\overleftrightarrow{N}_{ii}$ , as  $N_{ii}^{xx} = N_{ii}^{yy} = N$ , and  $N_{ii}^{zz} = N + \Delta N$ . In the case of PMR media, we can reasonably assume that the geometry of the grains is such that the axes for both the magnetostatic shape anisotropy and the crystal anisotropy terms will lie predominantly along the  $z$  axis, perpendicular to the film, with distributions characterized by a relatively small variance. As a consequence, the magnetostatic self-energy term and the crystal anisotropy can be combined into an effective single site uniaxial anisotropy with magnitude given by  $K_{\text{eff}} = K + \mu_0 \Delta N M_s^2/2$  and an axis aligned at an angle  $\alpha_{\text{eff}}$  to the  $z$  axis given by  $\tan \alpha_{\text{eff}}/\tan \alpha = 2K/(2K + \mu_0 \Delta N M_s^2)$ .

The introduction of the effective field into the energy expression Eq. (16), requires that after each grain reversal the system must be allowed to equilibrate before proceeding. Once the spin configuration and the effective fields have been determined self-consistently, the transition rate  $r_i = f_0 \exp(-\Delta E_i/k_B T)$  may be calculated for each grain. From this the wait time before the first reversal and the target spin can be obtained stochastically as before. The target spin is then flipped and the entire system is in a new state, which is then relaxed to give the new metastable equilibrium.

These steps are then repeated and the evolution of the system spin configuration due to thermally activated spin reversal is calculated.

To compare KMC with the finite-temperature LLG simulations we consider the decay of a uniformly magnetized film consisting of  $16 \times 16$  interacting grains of dimension  $8 \text{ nm} \times 8 \text{ nm} \times 10 \text{ nm}$  in a reverse field of magnitude  $H = 5 \text{ kOe}$ . The material parameters are  $M_s = 5 \times 10^5 \text{ A/m}$ ,  $A = 5 \times 10^{-12} \text{ J/m}$ ,  $K = 3.75 \times 10^5 \text{ J/m}^3$ ,  $\sigma_\alpha = 3^\circ$  and a damping parameter  $\alpha = 0.01$ . The attempt frequency for a SWP can be calculated explicitly in terms of the material parameters.<sup>34,38,39</sup> While the expressions of the attempt frequency obtained by various authors are similar, they nevertheless differ quantitatively reflecting the different approaches and approximations used in their derivation. For the present calculations the attempt frequency is calculated using the formula given in Ref. 39 in terms of the material parameters, LLG damping constant  $\alpha$ , and the gyromagnetic ratio  $\gamma$  as

$$f_0 = 2\alpha\gamma H_K \sqrt{\frac{4KV}{\pi k_B T}} \left(1 - \frac{H}{H_K}\right)^2 \quad (18)$$

with  $H = H_{\text{eff}}$ ,  $K = K_{\text{eff}}$ , and  $H_K = 2K_{\text{eff}}/M_s$  (results similar to those shown below are also obtained using Brown's formula<sup>34</sup>). Since  $f_0$  now involves the effective fields, the attempt frequency must be calculated for each individual grain and updated after each reversal. The results presented in Fig. 4 show good agreement between the two methods. Both show an approximately linear dependence of the magnetization on  $\ln t$  for  $t \gtrsim 0.1 \mu\text{s}$ .<sup>31</sup> In comparing the two curves in Fig. 4 it should be noted that the KMC results involve no adjustable parameters and that while the computational effort required to extend the results of the LLG simulations beyond  $10 \mu\text{s}$  is prohibitive, extending the calculation of the magnetization to hours or even years using KMC requires only a modest computational effort.

In Fig. 5 we present the results for the remanent coercivity obtained in the previous section for an ensemble of noninteracting SWPs together with results that include the magnetostatic and exchange interactions. In both cases we

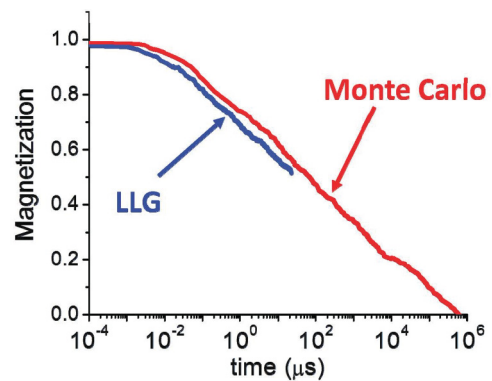


FIG. 4. (Color online) Time evolution of the magnetization per spin for a system of  $16 \times 16$  grains with  $M_s = 5 \times 10^5 \text{ A/m}$ ,  $A = 5 \times 10^{-12} \text{ J/m}$ ,  $K = 3.75 \times 10^5 \text{ J/m}^3$ ,  $\sigma_\alpha = 3^\circ$  for  $T = 330 \text{ K}$ . The LLG calculations were performed with a damping parameter  $\alpha = 0.01$ . For the KMC calculations the attempt frequency was calculated from Eq. (18).

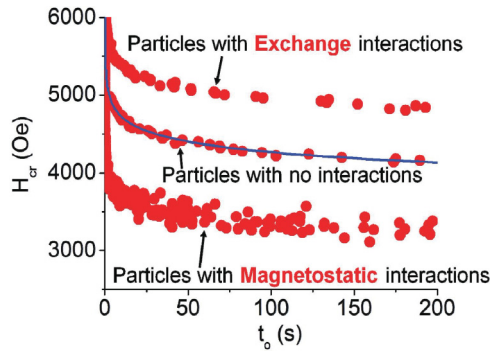


FIG. 5. (Color online) Remanent coercivity  $H_{cr}$  as a function of  $t_0$  for  $16 \times 16$  rectangular array of cells with dimensions  $8 \text{ nm} \times 8 \text{ nm} \times 10 \text{ nm}$  with  $M_s = 5 \times 10^5 \text{ A/m}$ ,  $K = 3.75 \times 10^5 \text{ J/m}^3$ , and  $\sigma_\alpha = 3^\circ$ , with and without interactions, as indicated on the figure. In both cases  $f_0 = 1 \text{ GHz}$  was assumed and, in the case of the exchange interaction,  $A = 5 \times 10^{-12} \text{ J/m}$  was used.

model the material as described above but treat the attempt frequency as constant with  $f_0 = 1 \text{ GHz}$ . These results show that the magnetostatic field significantly reduces the coercive field while the ferromagnetic exchange interaction increases  $H_{cr}$ .

#### IV. THERMAL DEGRADATION OF A BIT PATTERN

The methodology developed in the previous section can also be applied to consider the decay of a bit pattern due to thermally activated spin reversal. Figure 6 shows images of a synthetically generated bit pattern at various stages of decay. The initial pattern (approximately 7.5 grains per bit), shown in Fig. 6(a), was generated using the LLG simulations for a  $256 \times 32$  grid of cells of dimension  $6.2 \text{ nm} \times 6.2 \text{ nm} \times 20.0 \text{ nm}$  with  $M_s = 5.5 \times 10^5 \text{ A/m}$ ,  $K = 3.5 \times 10^5 \text{ J/m}^3$  and  $\sigma_\alpha = 3^\circ$  at  $T = 0$ . The subsequent time evolution was calculated using KMC at temperature of  $T = 450 \text{ K}$  with a constant attempt frequency  $f_0 = 100 \text{ GHz}$ . Each pixel in Fig. 6 represents a single grain.

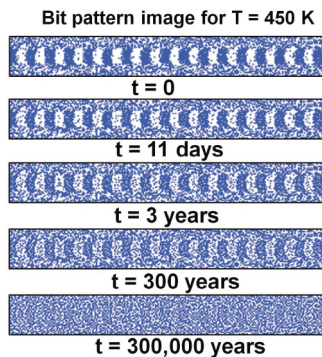


FIG. 6. (Color online) Evolution of a synthetic bit pattern calculated using KMC, with  $T = 450 \text{ K}$  and a constant attempt frequency  $f_0 = 100 \text{ GHz}$ . Each pixel represents a single grain with dimensions of  $6.2 \text{ nm} \times 6.2 \text{ nm} \times 20 \text{ nm}$ , a saturation magnetization of  $M_s = 5.5 \times 10^5 \text{ A/m}$  and an anisotropy constant of  $K = 3.5 \times 10^5 \text{ J/m}^3$ . The uniaxial anisotropy orientation is normally distributed about the perpendicular axis of the film with a variance  $\sigma_\alpha = 3^\circ$ .

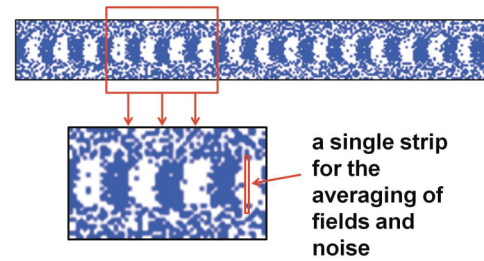


FIG. 7. (Color online) Schematic showing the strip of empty cells used to calculate the average perpendicular stray field detected by the transducer as it passes over the bit pattern.

The images presented in Fig. 6 clearly show the degradation of the bit pattern with time due to the thermally activated grain reversals. This degradation gives rise to a loss of signal over time and a decrease in the signal-to-noise ratio (SNR). To estimate the SNR we calculate the stray field in a narrow strip of empty cells aligned at right angles to the track shown in the inset included in Fig. 7. Assuming that the strength of the signal generated by the transducer will be proportional to the average of the perpendicular component of the field in the narrow strip we can calculate the bit field SNR in decibels as

$$\text{SNR} = 10 \ln \left( \frac{\sum_{\text{strip}} \langle H_z \rangle^2}{\sum_{\text{strip}} \langle H_z^2 \rangle - \langle H_z \rangle^2} \right) \text{ dB}. \quad (19)$$

The calculated values of the SNR in dB for 12 different runs are plotted as a function of the product  $f_0 t$  in Fig. 8 for four different temperatures ( $T = 300 \text{ K}$ ,  $T = 330 \text{ K}$ ,  $T = 350 \text{ K}$ , and  $T = 450 \text{ K}$ ) using three different attempt frequencies ( $f_0 = 1 \text{ GHz}$ ,  $f_0 = 10 \text{ GHz}$ , and  $f_0 = 100 \text{ GHz}$ ). The results show how the decrease in SNR over time depends very strongly on temperature as previously found for the case of longitudinal media.<sup>9</sup>

It is also useful to note that when the data are plotted as a function of  $f_0 t$  the results are independent of the attempt frequency  $f_0$ , which simply serves to determine the overall time scale. This rather trivial scaling suggests the possibility of a more general form of scaling based

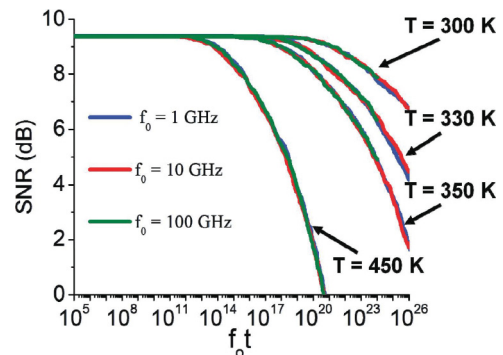


FIG. 8. (Color online) Bit pattern SNR calculated using Eq. (19) as a function of the product  $f_0 t$  for 12 different runs are plotted as a function of  $f_0 t$ . The runs consisted of four different temperatures ( $T = 300 \text{ K}$ ,  $T = 330 \text{ K}$ ,  $T = 350 \text{ K}$ , and  $T = 450 \text{ K}$ ) using three different attempt frequencies ( $f_0 = 1 \text{ GHz}$ ,  $f_0 = 10 \text{ GHz}$ , and  $f_0 = 100 \text{ GHz}$ ).

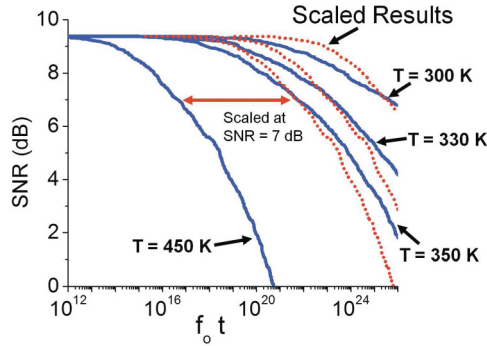


FIG. 9. (Color online) SNR vs  $f_0 t$  for the parameters and temperatures given in Fig. 8 (solid lines) and the results for  $T = 450$  K scaled according to the expressions given by Eqs. (20) and (21) (dotted lines).

on the assumption that  $\text{SNR}(T, t) = s[r(T)t]$ , where  $r(T)$  denotes some average transition rate for the system of the form  $r(T) = f_0 \exp(-\Delta E_{\text{eff}}/k_B T)$ , where  $f_0$  and  $\Delta E_{\text{eff}}$  are independent of the  $T$ . Defining  $t_1$  and  $t_2$  from the equation  $\text{SNR}(T_1, t_1) = \text{SNR}(T_2, t_2)$ , the effective energy barrier  $\Delta E_{\text{eff}}$  may be written as

$$\Delta E_{\text{eff}} = k_B \left( \frac{T_1 T_2}{T_2 - T_1} \right) \ln \left( \frac{t_1}{t_2} \right). \quad (20)$$

Using this scaling relation between the time and the temperature the SNR at any temperature  $T$  can be calculated from the SNR function at some reference temperature  $T_0$  since  $\text{SNR}(T, t) = \text{SNR}(T_0, t_0)$  with

$$t = t_0 \exp \left[ \frac{\Delta E_{\text{eff}}}{k_B} \left( \frac{1}{T_0} - \frac{1}{T} \right) \right]. \quad (21)$$

Figure 9 shows the SNR calculated using Eq. (21), with  $T_0 = 450$  K and  $\Delta E_{\text{eff}}$  calculated using Eq. (20), at  $\text{SNR} = 7$  dB for  $T_1 = 450$  K and  $T_2 = 350$  K. The poor agreement between the SNR curves obtained using the scaling law and the Monte Carlo results implies that any scaling relation relating time and temperature must be of a more complicated nature than that expressed by Eqs. (20) and (21).

## V. MH LOOPS AND THE SWEEP-RATE DEPENDENCE OF THE COERCIVE FIELD

In this section we study the sweep-rate dependence of finite-temperature  $MH$  loops calculated using KMC by considering the effect of an applied field that decreases in steps  $\Delta H$  of constant duration  $\Delta t$ . The KMC results are compared with those obtained using the finite-temperature LLG simulations. However, before presenting the results for finite temperature it is useful to first consider zero-temperature  $MH$  loops calculated using a variant of the KMC algorithm.

To study the  $MH$  loops for the  $T = 0$  case we consider the application of an initial perpendicular magnetic field, denoted by  $\vec{H}_0 = H_0 \hat{z}$ . The applied field is then varied in a sequence of steps of  $-\Delta H \hat{z}$  until  $\vec{H} = -\vec{H}_0$  is achieved. After each step the system is allowed to relax. At some point in the process the effective field acting on a particular grain will change direction so that it is now in a metastable equilibrium. As the magnitude of the applied field increases further, the effective field will equal

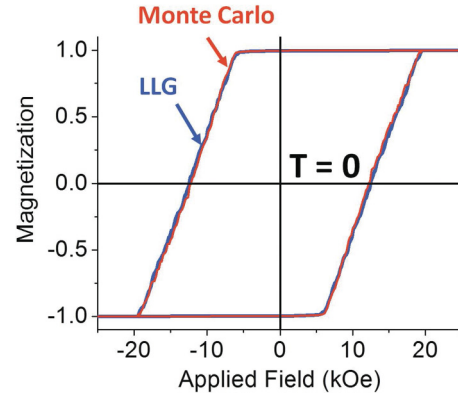


FIG. 10. (Color online) Zero-temperature  $MH$  loop for a system of  $16 \times 16$  grains of dimension  $6.2 \text{ nm} \times 6.2 \text{ nm} \times 20 \text{ nm}$  with  $M_s = 5.5 \times 10^5 \text{ A/m}$ ,  $K = 3.5 \times 10^5 \text{ J/m}^3$  and  $A = 5 \times 10^{-12} \text{ J/m}$  with  $\sigma_\alpha = 3^\circ$ . Data are shown for both LLG simulations and for the  $T \rightarrow 0$  limit of the KMC algorithm.

the switching field  $H_i^{\text{eff}} = H_s(\cos \theta_{\text{eff}})$  and the target grain will become unstable. This grain is reversed and the system equilibrated. Repeating this process can be regarded as the  $T \rightarrow 0$ ,  $r_i \rightarrow 0$  limit of the KMC algorithm. Figure 10 shows a comparison of zero-temperature  $MH$  loops obtained from this method and the equivalent results obtained from micromagnetics for a system of  $16 \times 16$  grains of dimension  $6.2 \text{ nm} \times 6.2 \text{ nm} \times 20 \text{ nm}$  with  $M_s = 5.5 \times 10^5 \text{ A/m}$ ,  $K = 3.5 \times 10^5 \text{ J/m}^3$ , and  $A = 5 \times 10^{-12} \text{ J/m}$  with  $\sigma_\alpha = 3^\circ$ . The results obtained from the two methods are in excellent agreement.

A similar procedure may be applied to study low-frequency hysteresis loops at finite temperature. As in the  $T = 0$  case the field is reduced by an amount  $\Delta \vec{H}$  in a sequence of steps of duration  $\Delta t$  until  $\vec{H} = -\vec{H}_0$ . The ratio  $R = \Delta H / \Delta t$  defines the sweep rate for the hysteresis loop. As the applied field is reduced and the system is allowed to relax, the grains which have a double energy minima are identified, and the energy barrier separating them is calculated. From this, the transition rates  $r_i$  together with the stochastic variables  $t_i = r_i^{-1} \ln x$  are calculated and the wait time  $T_w^{(1)} = \min\{t_i\}$  together with the target spin determined. If the wait time  $T_w^{(1)} > \Delta t$  then no change is made to the system, the magnitude of the applied field is reduced by an amount  $\Delta H$ , and the system is allowed to relax to a new metastable state. If on the other hand the wait time  $T_w^{(1)} < \Delta t$  the target spin is flipped and the system is allowed to relax to a new metastable state and the effective fields for each of the grains is calculated. The grains for which there exists a double energy minimum are identified and  $T_w^{(2)}$  calculated. If  $T_w^{(1)} + T_w^{(2)} > \Delta t$  then no change is made to the system and the magnitude of the applied field is reduced by an amount  $\Delta H$  and the system is allowed to relax to a new metastable state. If, on the other hand,  $T_w^{(1)} + T_w^{(2)} < \Delta t$  then we flip the target grain and repeat this process  $n$  times until  $T_w^{(1)} + T_w^{(2)} \dots + T_w^{(n)} > \Delta t$  at which point the magnitude of the field is reduced by an amount  $\Delta H$  and the system is relaxed to a new metastable state.

Figure 11 compares  $MH$  loops for several sweep rates calculated using KMC with those obtained from the finite-temperature LLG simulations. In the case of the LLG calculations a value of  $\alpha = 0.05$  is used, while for the KMC algorithm

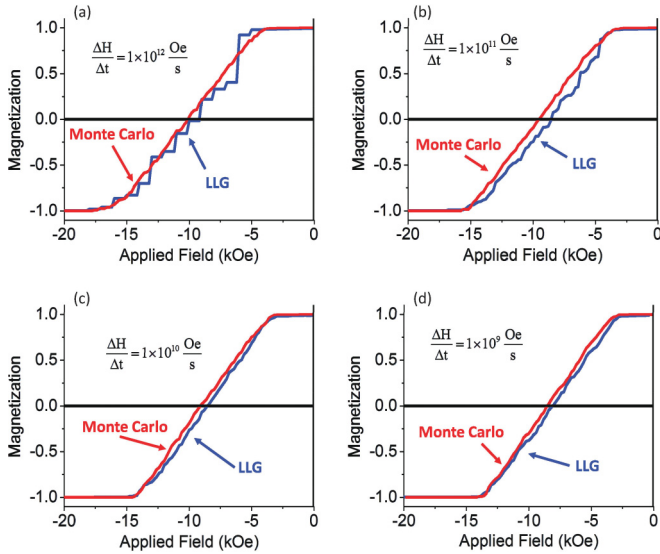


FIG. 11. (Color online)  $M$  vs  $H$  loops at  $T = 330$  K for an ensemble of  $16 \times 16$  grains of dimension  $6.2 \text{ nm} \times 6.2 \text{ nm} \times 20 \text{ nm}$  with  $M_s = 5.5 \times 10^5 \text{ A/m}$ ,  $K = 3.5 \times 10^5 \text{ J/m}^3$ , and  $A = 5 \times 10^{-12} \text{ J/m}$  with  $\sigma_\alpha = 3^\circ$ . Data are shown for both LLG simulations, with  $\alpha = 0.1$  and KMC, with  $f_0 = 50 \text{ GHz}$  for  $\Delta H/\Delta t =$  (a)  $1 \times 10^{12} \text{ Oe/s}$ , (b)  $1 \times 10^{11} \text{ Oe/s}$ , (c)  $1 \times 10^{10} \text{ Oe/s}$ , and (d)  $1 \times 10^9 \text{ Oe/s}$ .

$f_0$  is again calculated using Eq. (18). At the highest sweep rate  $R = 1 \times 10^{12} \text{ Oe/s}$  [Fig. 11(a)] there is a significant difference in the results obtained between the two methods reflecting the dominance of the dynamics in the reversal process in this regime that is captured in the LLG simulations but which is not accounted for in KMC, which is based simply on the energetics of the grain reversal process. As the sweep rate is reduced Figs. 11(b)–11(d) show that the differences between the two methods decrease, with good agreement between the two methods in Fig. 11(d).

$MH$  loops calculated for  $T = 330$  K using KMC with sweep rates ranging from  $1 \times 10^{12} \text{ Oe/s}$  to  $1 \times 10^6 \text{ Oe/s}$  are shown in Fig. 12 together with the corresponding results

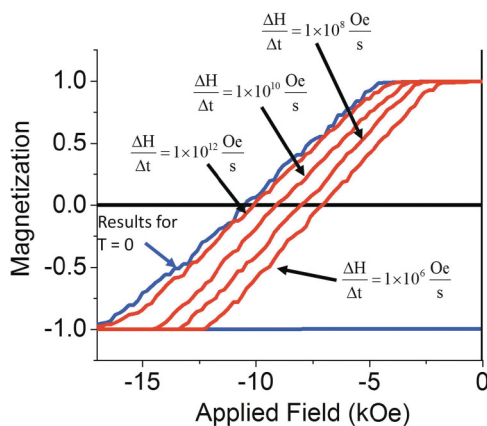


FIG. 12. (Color online)  $M$  vs  $H$  at  $T = 300$  K for several sweep rates for a  $16 \times 16$  ensemble of grains of dimension  $6.2 \text{ nm} \times 6.2 \text{ nm} \times 20 \text{ nm}$  with  $M_s = 5.5 \times 10^5 \text{ A/m}$ ,  $K = 3.5 \times 10^5 \text{ J/m}^3$ , and  $A = 5 \times 10^{-12} \text{ J/m}$  with  $\sigma_\alpha = 3^\circ$ , calculated using KMC with  $f_0 = 50 \text{ GHz}$ . The  $T = 0$   $MH$  loop is included for comparison.

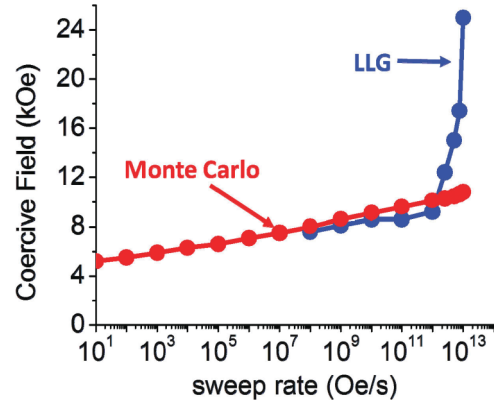


FIG. 13. (Color online) Coercive field as a function of sweep rate calculated from  $MH$  loops shown in Fig. 12 together with corresponding results calculated using finite-temperature LLG simulations with  $\alpha = 0.1$ . The discrepancy at the lowest sweep rates is attributed to approximations in the estimate of the attempt frequency.

for  $T = 0$ . The results illustrate the expected decrease in the coercive field  $H_c$  with decreasing sweep rate due to the effects of thermally assisted grain reversal. The coercivity calculated from the finite-temperature  $MH$  loops is plotted in Fig. 13 as a function of sweep rate together with the results obtained from the finite temperature LLG simulations. Due to the computational requirements of the LLG calculations the data only extend down to a sweep rate of  $10^8 \text{ Oe/s}$  whereas the KMC data extend down to  $10^{-1} \text{ Oe/s}$ .

There are a number of aspects of the results presented in Fig. 13 that deserve comment. As noted previously, the coercive field calculated using the LLG data shows a sharp upturn at the highest sweep rates. A similar upturn has been seen in related simulation results.<sup>12</sup> In addition, we note that while the two methods show good agreement at the lower values of  $R$ , there remains a very small discrepancy. We attribute these differences to the approximations used in estimating  $f_0$  from Eq. (20), which is likely exacerbated by the high aspect ratio of the grains.<sup>42</sup> The ability of the KMC algorithm to simulate  $MH$  loops with a very low sweep rate is of considerable importance in modeling the properties of magnetic materials using data obtained at frequencies relevant to experimental VSM measurements.

## VI. SUMMARY AND CONCLUSIONS

We have applied a variant of KMC, commonly referred to as the FRM, to study thermally assisted grain reversal in PMR media. The basis of the FRM is the calculation of the sequence of successive grain reversals and the time between them as defined by the minimum of the stochastic time variables  $t_i$  given by Eq. (14) in terms of the transition rates  $r_i$  for the individual grains. The FRM is the KMC variant of choice in the case of time-dependent transition rates.<sup>22,23</sup> The similarities with earlier work<sup>30</sup> in applying KMC to primarily longitudinal media are discussed.<sup>29–33</sup>

The transition rates are calculated using the Arrhenius-Néel expression using an analytical expression for the location of the maxima and minima of the energy of a SWP.<sup>21</sup>

This allows the minimum-energy alignment of the magnetic moments and the energy barriers separating them to be readily determined. The stochastic nature of the procedure reflects the process of punctuated equilibrium that describes the effect of the thermally activated grain reversals and also satisfies the principle of detailed balance. The method is used to calculate the remanent coercivity for an ensemble of noninteracting SWPs and gives excellent agreement with the analytic results obtained from the direct integration of the rate equations (Sharrock's Law).

Generalizing KMC to include the magnetostatic and exchange interactions between the grains requires that the energy of the SWPs be modified to include the magnetostatic shape anisotropy and the applied field replaced by an effective field that includes both the exchange and long-range magnetostatic fields. The effective fields and the magnetic-moment vector of the individual grains are calculated self-consistently and the system can be allowed to relax to a metastable state following a grain reversal.

In order to compare the results of a system of interacting grains calculated using KMC with the finite-temperature LLG simulations, the attempt frequency is calculated using the formula given in Eq. (18) that includes an explicit dependence on both the temperature and the effective field acting on the individual grains. Results for the decay of a uniformly magnetized film in a reverse field calculated using KMC show good agreement with those obtained from the LLG simulations over time scales  $\sim 10 \mu\text{s}$ . Of particular note is the fact that while the LLG calculations required in excess of 50 h of CPU time, the corresponding KMC calculations took only a matter of minutes and could be extended out to much longer times scales with only a modest computational effort. The calculation of the remanent coercivity was also generalized to examine the effects of the magnetostatic and exchange interactions on the remanent coercivity.

Kinetic Monte Carlo was also applied to model the decay of a bit pattern due to thermally activated grain reversal over periods of several years. Results showing degradation of the signal-to-noise ratio of the bit pattern over time were presented for several different temperatures and attempt frequencies. It is also shown how KMC may be generalized to study the application of time-dependent magnetic fields. This is used to model *MH* loops at finite temperature and to study the dependence of the coercive field on sweep rate. The attempt

frequency is again calculated using Eq. (18) and the results compared with those obtained from the finite-temperature LLG simulations. A comparison of the results obtained from the two methods shows that while the agreement is poor for very high sweep rates the agreement between the two methods for lower sweep rates  $10^8 \text{ Oe/s} < R < 10^{12} \text{ Oe/s}$  is very good. The discrepancy at higher sweep rates may be attributed to the dominance of dynamical switching as captured by the LLG simulations. The obvious advantage of KMC is that it can calculate the coercive field for sweep rates of relevance to experimental VSM measurements, that are many orders of magnitude less than what can be realistically calculated using the finite-temperature LLG simulations.

In addition to demonstrating the ability of KMC to successfully model single domain, highly anisotropic weakly interacting grains over time scales that can extend to millennia, the present work also demonstrates that KMC provides a framework to study magnetic materials that are dominated by energetics and thermal activation and whose evolution can be characterized by a sequence of abrupt transitions between of long-lived metastable equilibrium states. Unlike the more conventional LLG simulations that can be applied to give detailed dynamical information for a wide range of problems, the Monte Carlo approach instead focusses on evaluating the time between successive grain reversals and their effect on the net magnetization. This shifts the emphasis from modeling the dynamics of a system to identifying the metastable states of the individual grains and determining the transition rates between them. As such, the method can be readily generalized to include other forms of anisotropy<sup>43</sup> as well as attempt frequencies<sup>39,42</sup> and energy barriers<sup>44</sup> associated with the more complex structure of multilayer ECC media. While extending the KMC algorithm to include such effects could significantly increase the computational burden, the determination of the  $N$  stochastic variables  $t_i$  are essentially independent tasks and therefore well suited to parallel computation.

#### ACKNOWLEDGMENTS

This work was supported by Western Digital Corporation, the Natural Science and Engineering Research Council (NSERC) of Canada, the Canada Foundation for Innovation (CFI), and the Atlantic Computational Excellence network (ACEnet).

<sup>1</sup>M. Plumer, J. v. Ek, and W. Cain, *Phys. Can.* **67**, 25 (2011).

<sup>2</sup>H. J. Richter, A. Lyberatos, U. Nowak, R. F. L. Evans, and R. W. Chantrell, *J. Appl. Phys.* **111**, 033909 (2012).

<sup>3</sup>H. J. Richter, *J. Phys. D* **40**, R149 (2007).

<sup>4</sup>D. Suess, J. Lee, J. Fidler, and T. Schrefl, *J. Magn. Magn. Mater.* **321**, 545 (2009).

<sup>5</sup>J. I. Mercer, M. L. Plumer, J. P. Whitehead, and J. van Ek, *Appl. Phys. Lett.* **98**, 192508 (2011).

<sup>6</sup>T. A. Ostler, J. Barker, R. F. L. Evans, R. W. Chantrell, U. Atxitia, O. Chubykalo-Fesenko, S. El Moussaoui, L. Le Guyader, E. Mengotti, L. J. Heyderman *et al.*, *Nat. Commun.* **3**, 666 (2012).

<sup>7</sup>T. W. McDaniel, *J. Appl. Phys.* **112**, 013914 (2012).

<sup>8</sup>Y. Shiroishi, K. Fukuda, I. Tagawa, H. Iwasaki, S. Takenoiri, H. Tanaka, H. Mutoh, and N. Yoshikawa, *IEEE Trans. Mag.* **45**, 3816 (2009).

<sup>9</sup>*The Physics of Ultra-High-Density Magnetic Recording*, edited by M. L. Plumer, J. v. Ek, and D. Weller (Springer-Verlag, Berlin, 2001).

<sup>10</sup>E. C. Stoner and E. P. Wohlfarth, *Philos. Trans. R. Soc. A* **240**, 599 (1948).

<sup>11</sup>W. Brown, *Phys. Rev.* **130**, 1677 (1963).

- <sup>12</sup>M. L. Plumer, M. D. Leblanc, J. P. Whitehead, and J. van Ek, *J. Appl. Phys.* **111**, 123905 (2012).
- <sup>13</sup>J. Xue and R. H. Victora, *Appl. Phys. Lett.* **77**, 3432 (2000).
- <sup>14</sup>J. Xue and R. H. Victora, *J. Appl. Phys.* **89**, 6985 (2001).
- <sup>15</sup>M. P. Sharrock and J. T. McKinney, *IEEE Trans. Mag.* **17**, 3020 (1981).
- <sup>16</sup>X. Feng and P. B. Visscher, *J. Appl. Phys.* **95**, 7043 (2004).
- <sup>17</sup>Y. Zhang and H. N. Bertram, *IEEE Trans. Mag.* **34**, 3786 (1998).
- <sup>18</sup>A. Moser and D. Weller, *IEEE Trans. Mag.* **35**, 2808 (1999).
- <sup>19</sup>In the present context the acronym FRM should more appropriately refer to the “first reversal method.”
- <sup>20</sup>D. T. Gillespie, *J. Comput. Phys.* **22**, 403 (1977).
- <sup>21</sup>R. Wood, *IEEE Trans. Mag.* **45**, 100 (2009).
- <sup>22</sup>A. P. J. Jansen, *Chem. Phys. Lett.* **86**, 1 (1995).
- <sup>23</sup>V. Rai, H. Pitsch, and A. Novikov, *Phys. Rev. E* **74**, 046707 (2006).
- <sup>24</sup>I. Martin-Bragado, S. Tian, M. Johnson, P. Castrillo, R. Pinacho, J. Rubio, and M. Jaraiz, *Nucl. Instrum. Methods Phys. Res., Sect. B* **253**, 63 (2006).
- <sup>25</sup>T. Opplestrup, V. V. Bulatov, G. H. Gilmer, M. H. Kalos, and B. Sadigh, *Phys. Rev. Lett.* **97**, 230602 (2006).
- <sup>26</sup>A. Chotia, M. Viteau, T. Vogt, D. Comparat, and P. Pillet, *New J. Phys.* **10**, 045031 (2008).
- <sup>27</sup>T. Franz and F. Mittendorfer, *J. Chem. Phys.* **132**, 194701 (2010).
- <sup>28</sup>D. T. Gillespie, *Chem. Phys. Lett.* **81**, 2340 (1977).
- <sup>29</sup>R. W. Chantrell, A. Lyberatos, and E. P. Wohlfarth, *J. Phys. F* **16**, L145 (1986).
- <sup>30</sup>Y. Kanai and S. H. Charap, *IEEE Trans. Mag.* **27**, 4972 (1991).
- <sup>31</sup>P.-L. Lu and S. H. Charap, *J. Appl. Phys.* **75**, 5768 (1994).
- <sup>32</sup>S. H. Charap, P.-L. Lu, and Y. He, *IEEE Trans. Mag.* **33**, 978 (1997).
- <sup>33</sup>Y. Uesaka, Y. Takahashi, Y. Nakatani, N. Hayashi, and H. Fukushima, *J. Magn. Magn. Mater.* **174**, 203 (1997).
- <sup>34</sup>W. F. Brown, *Phys. Rev.* **130**, 1677 (1963).
- <sup>35</sup>D. C. Crew, P. G. McCormick, and R. Street, *J. Appl. D: Appl. Phys.* **29**, 2313 (1996).
- <sup>36</sup>H. N. Bertram Fellow, X. Wang, and V. L. Safonov, *IEEE Trans. Mag.* **37**, 1521 (2001).
- <sup>37</sup>E. Wernsdorfer, E. Bonet Orozco, K. Hasselbach, A. Benoit, B. Barbara, N. Demoncy, A. Loiseau, H. Pascard, and D. Mailly, *Phys. Rev. Lett.* **78**, 1791 (1997).
- <sup>38</sup>V. L. Safonov, *J. Magn. Magn. Mater.* **195**, 523 (1999).
- <sup>39</sup>X. Wang and H. N. Bertram, *J. Appl. Phys.* **92**, 4560 (2002).
- <sup>40</sup>L. Breth, D. Suess, C. Vogler, B. Bergmair, M. Fuger, R. Heer, and H. Brueck, *J. Appl. Phys.* **112**, 023903 (2012).
- <sup>41</sup>In all subsequent discussion KMC refers to the FRM variant of the KMC algorithm unless otherwise stated.
- <sup>42</sup>G. Fiedler, J. Fidler, J. Lee, T. Schrefl, R. L. Stamps, H. B. Braun, and D. Suess, *J. Appl. Phys.* **111**, 093917 (2012).
- <sup>43</sup>A. Tamion, E. Bonet, F. Tournus, C. Raufast, A. Hillion, O. Gaier, and V. Dupuis, *Phys. Rev. B* **85**, 134430 (2012).
- <sup>44</sup>R. Dittrich, T. Schrefl, D. Suess, W. Scholz, H. Forster, and J. Fidler, *J. Magn. Magn. Mater.* **250**, L12 (2002).